Global NEST Journal, Vol 16, No 6, pp 1111-1120, 2014

SYNTHESIS, CHARACTERISATION AND CATALYTIC PERFORMANCE OF Cu- AND Co-MODIFIED Fe-Al CO-PRECIPITATED CATALYSTS FOR THE STEAM REFORMING OF ETHANOL

SOUZA G.[1,2]
RUOSO C.[1]
MARCILIO N.R.[1]
PEREZ-LOPEZ O.W.[1,*]

[1]*Department of Chemical Engineering*
Federal University of Rio Grande do Sul - UFRGS
R. Eng. Luiz Englert S/N° - Build. 12204, Porto Alegre, Brazil
[2]*Fundação de Ciência e Tecnologia do Estado do Rio Grande do Sul - CIENTEC*
Av. das Indústrias, 2270, Distrito Industrial, 94930-230 Cachoeirinha, Brazil

Received: 25/07/2014
Accepted: 16/10/2014
Available online: 17/12/2014

*to whom all correspondence should be addressed:
e-mail: perez@enq.ufrgs.br

ABSTRACT

This paper reports the synthesis and the investigation of the properties and performance of Fe-Al catalysts modified with Cu or Co for the steam reforming of ethanol. The materials were prepared by the precipitation method with different Fe/Al ratios. The samples were characterised by the S_{BET}, TG/DTG, XRD, H_2-TPR and TPO/DTA analyses. The increase in the Fe/Al ratio leads to a decrease in the specific surface area and shifts the reduction peaks towards higher temperatures. The partial substitution of Fe by Co or Cu modifies the structure of the materials because higher specific surface areas and crystallites of iron oxides with smaller sizes are formed. The promotion also improves the reducibility of the iron species. These changes provide higher activity and selectivity towards H_2 and CO for the modified samples and for the samples with lower Fe/Al ratio. The Co-containing catalyst showed the best performance because this sample exhibited the highest conversions and selectivity towards both H_2 and CO and the lowest formation of coke according to the TPO analysis.

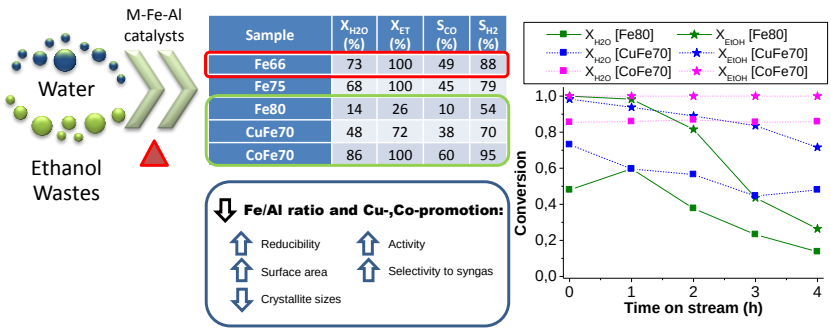

Keywords: Iron catalyst, precipitation method, mixed oxides, steam reforming, cobalt, copper, coke.

1. Introduction

The processes involving wastes derived from biomass feedstock arise as interesting alternatives taking into account the needs for the minimisation of landfill disposal and the depletion of the crude petroleum reserves and consequently oscillation on its price (de Souza *et al.*, 2012a; Ponton Lozano *et al.*, 2014). The steam reforming of bio-wastes is a promising route because it can originates hydrogen and synthesis gas (a mixture of H_2 and CO) from renewable resources. The use of hydrogen for fuel cells still requires greater efforts in terms of research and development before large scale application of this

technology. The questions related to the cost of this new infrastructure and the efficiency matters that would be required for a future hydrogen society could lead to the production of synthetic liquid fuels instead of only hydrogen (Huber *et al.*, 2005; Rostrup-Nielsen, 2005). Hydrocarbons and a wide range of other chemicals can be produced from the conversion of synthesis gas originated from biomass resources (such as rich ethanol wastes) through the Fischer-Tropsch Synthesis (FTS) or processes involving the synthesis and further transformation of methanol. Moreover, the FTS technology produces ultra clean diesel oil fraction with high cetane number and without any sulfur and aromatic compounds (Lira *et al.*, 2008), thus preventing the emission of pollutants such as particulates, benzene, toluene, polycyclic aromatic hydrocarbons (PAH) and SO_x.

The development of catalysts is crucial for the feasibility of the steam reforming of ethanol for commercial scale. Several catalysts have already been studied, mostly based on Ni (Zhang *et al.*, 2009a; Wang and Wang, 2010), Co (Song *et al.*, 2011; Espinal *et al.*, 2012; Davidson *et al.*, 2013) or noble metals such as Ir, Rh and Pd (Galvita *et al.*, 2001; Zhang *et al.*, 2008a; González Vargas *et al.*, 2013; Coronel *et al.*, 2014). However, nickel is still the preferred option because of its high activity for the reforming reaction and lower price (Dias and Assaf, 2003; Jones *et al.*, 2008). The literature does not report results for steam reforming of ethanol over Fe-based catalysts. However, its' much cheaper price (Dry, 2002), apparently moderate activity for reforming (Jones *et al.*, 2008) and interesting results involving the decomposition of ethanol (Li *et al.*, 2008; Wang *et al.*, 2011) are incentives to the investigation of Fe-bulk materials for the steam reforming of ethanol reaction.

This paper reports the study of Fe-Al catalysts for the steam reforming of ethanol, herein representing rich ethanol wastes. The samples were prepared by the precipitation method with different Fe/Al ratios. Also, the modifications on the structure and catalytic performance provided by the partial substitution of Fe^{3+} by a divalent metal (Cu^{2+} or Co^{2+}) was investigated in this work.

2. Methods

2.1 Preparation of samples

The samples were synthesised with different Fe/Al molar ratios by the continuous co-precipitation method described earlier (de Souza *et al.*, 2012a). The Fe-Al samples were prepared from an aqueous solution containing the Fe(III) and Al(III) nitrates. The aqueous solutions for the modified samples also contained the Co(II) or Cu(II) nitrates. An aqueous solution containing NaOH and Na_2CO_3 (1:1 v/v) was used as the precipitant. The solutions were continuously fed into a continuous stirred tank reactor (CSTR) kept at constant temperature (60 ± 1°C) and pH (9 ± 0.1). After crystallisation at 60°C for 1 h, the precipitate was filtered and washed with distilled and deionised water. After drying at 80°C for 24 h in an oven, the samples were crushed and sieved. The fraction with particle sizes between 355 and 500 μm was taken. The thermal treatment was conducted under an air flow of 50 mL min^{-1} at 600°C for 6 h.

2.2 Catalytic evaluation

The catalysts were reduced in situ under 100 mL min^{-1} of pure H_2 flow for 1 h at 600 °C prior to the catalytic evaluation. The steam reforming reactions were performed in a quartz tubular fixed bed reactor (6 mm i.d.) loaded with 100 mg of catalyst. The tests were performed under atmospheric pressure at 600°C. The flow rate of nitrogen was adjusted to 100 mL min^{-1} through a mass flow controller. The ethanol-water mixture (1:1 molar ratio) was fed by a syringe-type micro-pump at a flow rate of 0.5 mL h^{-1}. The products were analysed by gas chromatography. The ethanol conversion and the water consumption (X_{react}) were defined based on the concentration in the inlet ($[React]_{IN}$) and outlet ($[React]_{OUT}$) streams:

$$X_{react}(\%) = \frac{[React]_{IN} - [React]_{OUT}}{[React]_{IN}} \times 100 \quad (1)$$

The selectivity for hydrogen (S_{H2}) and C-containing products (S_{Ci}) was evaluated as follows:

$$S_{H_2} = \frac{[H_2]}{\sum v_j [H_{2j}]} \quad (2)$$

$$S_{C_i} = \frac{v_i [C_i]}{\sum v_j [C_j]} \quad (3)$$

Where $[C_j]$ and $[H_{2j}]$ is respectively the number of moles of C-containing and H_2-containing *j* product in the outlet stream and *υj* is the ratio of stoichiometric reaction coefficients.

2.3 Characterisation

The uncalcined samples were characterised by thermogravimetry (TG/DTG). The specific surface area (S_{BET}), X-ray diffraction (XRD) and temperature-programmed reduction (H_2-TPR) was performed for the calcined catalysts. The spent catalysts were investigated by the temperature-programmed oxidation coupled with differential thermal analyses (TPO/DTA).

The TG/DTG and TPO/DTA experiments were conducted using a thermobalance (TA Model SDT600). Approximately 10 mg each of the uncalcined (TG/DTG) or the spent sample (TPO/DTA) was purged with 1000 mL min^{-1} of nitrogen at 30°C for 10 min before the tests. Then the samples were heated at 10°C min^{-1} to 850°C under a synthetic air flow rate of 100 ml min^{-1}.

The S_{BET} and H_2-TPR data were collected using a multipurpose system equipped with a thermal conductivity detector (TCD). A quartz "U-type" reactor was loaded with 100 mg of the calcined sample and placed in a temperature-controlled oven. A pretreatment step under nitrogen flow at 250°C was conducted for 1 h before the measures. For the H_2-TPR analysis, the temperature was increased at a rate of 10°C min^{-1} from 40°C to 900°C. The heating was carried out under 30 ml min^{-1} of a diluted H_2/N_2 mixture (10% v/v). The S_{BET} data was recorded using the N_2 dynamic adsorption method at -196°C.

The XRD patterns were obtained using the powder method for the calcined catalysts. The patterns were collected for 2θ between 10 and 70° with a Bruker D2 Phaser X-ray diffractometer. The spectra were collected at ambient temperature using CuKα radiation.

3 Results and discussion

Table 1 exhibits the nominal molar composition and the S_{BET} measurements for the calcined catalysts.

Table 1. Nominal composition and S_{BET} measurements for the calcined samples

Sample	Composition (mol. %)				S_{BET} (m^2 g^{-1})
	Cu	Co	Fe	Al	
Fe66	0.0	0.0	66.7	33.3	79
Fe75	0.0	0.0	75.0	25.0	46
Fe80	0.0	0.0	80.0	20.0	37
CuFe70	10.0	0.0	70.0	20.0	78
CoFe70	0.0	10.0	70.0	20.0	78

Table 1 shows that the specific surface area strongly decreases with decreasing Al content for samples with different Fe/Al ratios. This trend highlights the role of aluminium as a structural promoter for the precipitated samples. Despite involving another metal with different oxidation state, the same behaviour was observed for Co-Al precipitated catalysts (Hermes, 2010). The substitution of 10 mol. % of iron by copper or cobalt significantly increases the specific surface area. The combination of both trivalent elements (Fe^{3+} and Al^{3+}) probably does not provide the formation of mixed oxides, which are known to possess high specific surface area. On the other hand, the presence of the divalent metals (Cu^{2+} or Co^{2+}) would allow the formation of mixed oxides, thus the increment on the specific surface

area provided by referred metals. Additionally, the presence of copper was told to lead to smaller crystallites of Fe_2O_3, which could also contribute to increase the specific surface area (Wan *et al.*, 2008).

Figure 1 exhibits the curves related to the thermal decomposition of the uncalcined Fe-Al samples.

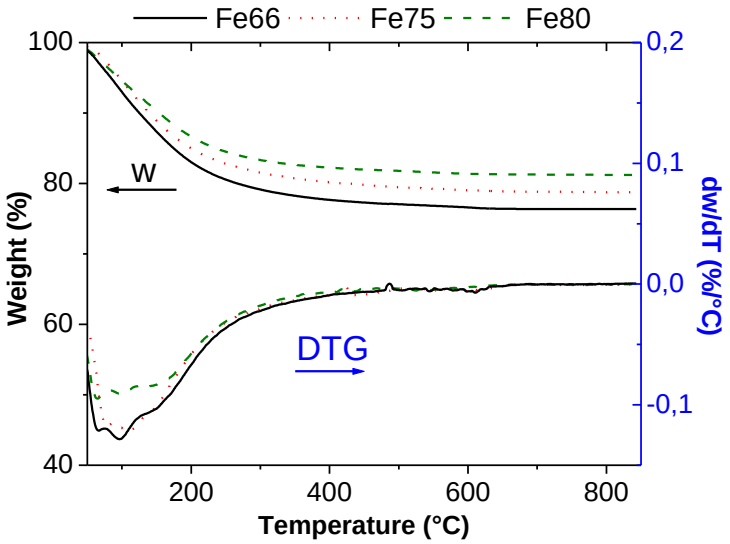

Figure 1. TG/DTG curves for uncalcined samples

The DTG peaks related to the decomposition of the precursors are observed at temperatures below 400°C. The decomposition phenomena might include the water removal at lower temperatures, followed by the release of the NO, OH^- and CO_3^{2-} compounds generated from the decomposition of the precursors (Crepaldi *et al.*, 2000; Frost *et al.*, 2005; Palmer *et al.*, 2009; Hermes *et al.*, 2011). The total weight loss in Figure 1 varied with the content of iron and aluminium on samples. However, the DTG peaks end at similar temperatures, suggesting that the thermal stability of the Fe-Al samples might be approximately the same. Other materials synthesised by the precipitation method with metal nitrates and sodium precursors also exhibited the thermal decomposition ending at temperatures below 400°C (Zhang *et al.*, 2008b; Hermes *et al.*, 2011).

The X-ray diffractograms and the H_2-TPR profiles for the calcined samples are showed in Figure 2-a and 2-b, respectively. The XRD patterns in Figure 2-a present diffraction reflections located at 2θ = 24.2, 33.2, 35.6, 40.9, 49.5, 54.0, 57.6, 62.4 and 64.0° for all the samples. These diffraction peaks can be ascribed to the hematite phase (Fe_2O_3). The X-ray diffraction patterns did not point to the formation of the hercynite phase ($FeAl_2O_4$). The diffractograms are similar to those reported by Zhang *et al.* (2009b) for Fe-Al materials prepared by the sol-gel method.

The CoFe70 present an additional reflection with weak intensity at 2θ = 36.9° that indicates the presence of the Co_3O_4 phase. Regarding the CuFe70 catalyst, the stronger peak ascribed to the tenorite phase (CuO) at 2θ = 38.7° was not identified in Figure 2-a, neither the reflections associated to Cu-containing mixed oxides. The additional phases expected for the CoFe70 and CuFe70 catalysts could not be precisely identified due to the low content of cobalt or copper on these samples. However, the absence of the aluminium ferrite is in agreement with the specific surface area measurements (Table 1), because the partial substitution of Fe by Cu or Co might form the mixed oxides that would lead to the increase in the surface area.

Based on the width at half the maximum intensity for the reflection at 2θ = 35.6°, a decrease in the crystallinity of the Fe_2O_3 phase is noted for both the Cu- and Co-modified catalysts compared to the Fe80 sample. This peak could also suggest that the partial substitution of Fe by Cu or Co originates Fe_2O_3 crystallites with smaller diameters, which would also be expected by the mixed oxides that might be formed for these modified samples.

The H_2-TPR curves are shown in Figure 2-b. Two main reduction peaks can be seen for all the Fe-Al samples. The peaks located at temperatures in the range 300-550°C can be ascribed to the reduction of the Fe_2O_3 phase to the Fe_3O_4 phase and possibly its subsequent reduction to FeO. The overlapped peaks starting at 600°C are related to further transformations of the iron oxides to metallic iron. This peak at higher temperatures could also be related to the reduction of the $FeAl_2O_4$ spinel phase because the mixed oxides are told to be thermally more stable and therefore more difficult to be reduced (Vaccari, 1998; Hermes *et al.*, 2011). Nonetheless, this Fe-Al mixed oxide phase was not identified by the XRD analysis (Figure 2-a) and is not expected from the iron precursor adopted (Fe^{3+}). The peak at higher temperatures does not finish due to the limit of the equipment for the upper temperature. However, it can be seen that the reduction peaks shift towards higher temperatures with increasing Fe/Al ratio. The reduction profile found for the Fe-Al samples is similar to that reported for other bulk iron (Hayakawa *et al.*, 2006) and Fe-Al materials (Oliveira and Rangel, 2003).

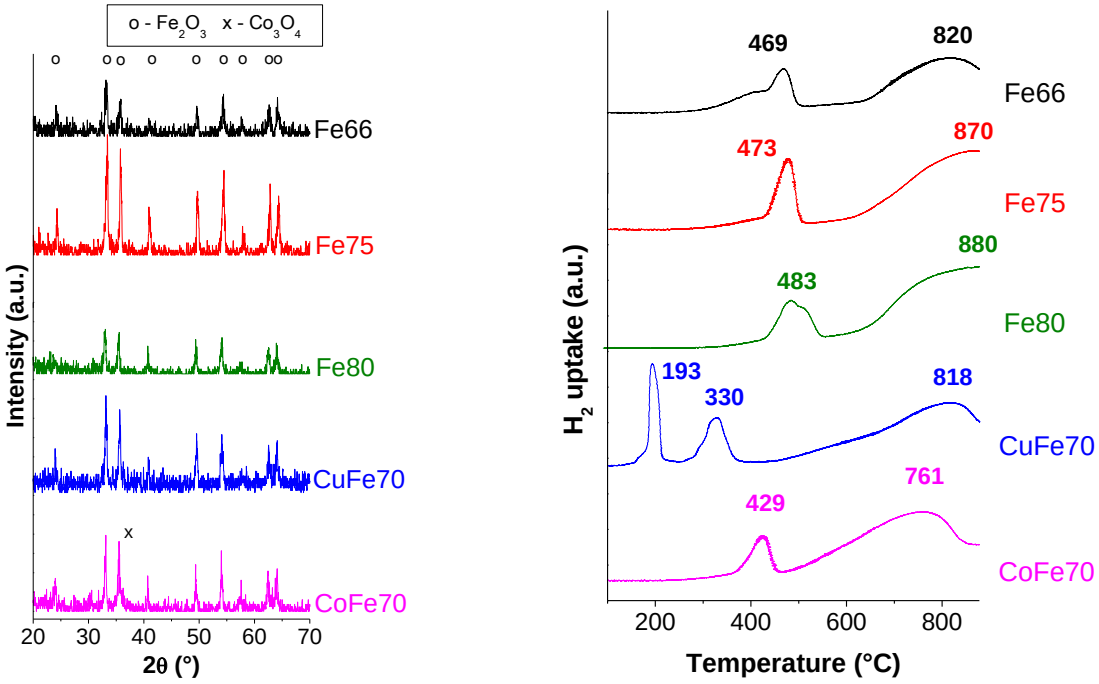

Figure 2. (a) XRD patterns and (b) H_2-TPR profiles for calcined samples

For the CoFe70 catalyst, two main peaks are also observed. The first one takes place at approximately the same temperature compared to the unpromoted Fe-Al samples. This peak is ascribed to the reduction of the Fe_2O_3 and the bulk cobalt oxides to metallic cobalt. The reduction of Co_3O_4 to Co^0 is known to takes place at these temperatures. Additionally to the further reduction of the iron oxides to metallic iron, the hydrogen consumption at higher temperatures might also include the reduction of the $CoAl_2O_4$ phase identified by the XRD analysis (Figure 2-a) (Hermes *et al.*, 2011; Cai *et al.*, 2013; Escobar and Perez-Lopez, 2014; Fakeeha *et al.*, 2014).

The copper-promoted catalyst show a different reduction profile compared to the other catalysts. An additional peak is noted at temperatures in the range 135 – 230 °C. This TPR peak is assigned to the reduction CuO to Cu^0. The peak attributed to the initial reduction of the Fe_2O_3 phase occurs at lower temperatures for the CuFe70 sample. As showed in other papers, the presence of copper shifts the reduction of the iron oxides towards lower temperatures. The Cu crystallites nucleate during reduction of CuO at lower temperatures, providing H_2 dissociation sites capable of reducing iron oxides at significantly lower temperatures (Zhang *et al.*, 2006; Wan *et al.*, 2008). The addition of copper also shifts

significantly towards lower temperatures the further reduction of the iron oxides to Fe^0 and possibly the reduction of the Cu-containing mixed oxides. For example, this broad reduction peak starts at *ca*. 100°C lower temperatures compared to the Fe66 sample. The same behaviour was observed for the Cu-Co-Al mixed oxides reported by Escobar and Perez-Lopez (2014).

Figure 3 exhibits the variation of the distribution of products and water consumption with time on stream for the steam reforming of ethanol over the Fe66 catalyst. The conversion of ethanol was complete during all the reaction.

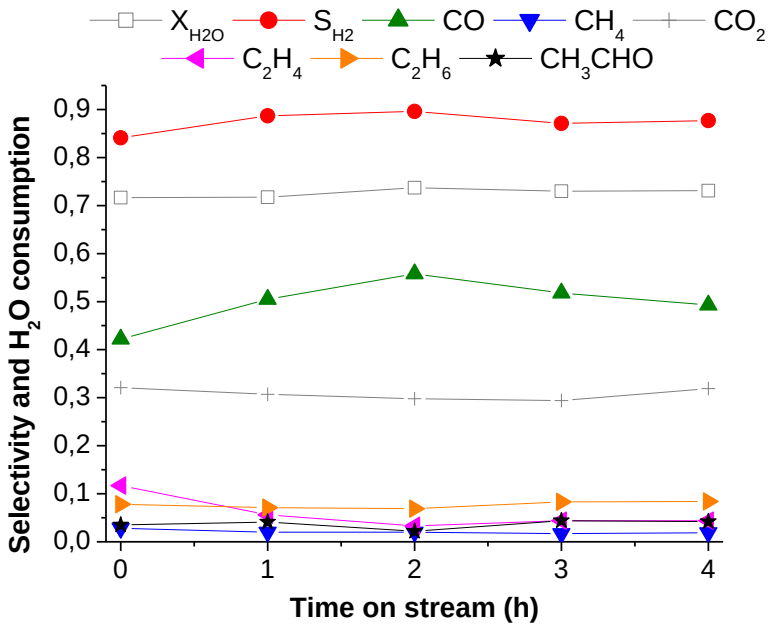

Figure 3. Distribution of products and water consumption with time on stream for the steam reforming of ethanol over the Fe66 catalyst

As illustrated in Figure 3 for the Fe66 catalyst, the distribution of products and the water consumption did not change significantly during the catalytic evaluation. For the Fe66 catalyst, the highest selectivity values towards hydrogen and carbon monoxide and consumption of water was observed after 2 h, although it remains almost at the same level in the period range 2 – 4 h. The main products formed during the reaction are H_2, CO and CO_2. This result highlights the steam reforming of ethanol reactions (eq. 4 and eq. 5) that are favoured during all the catalytic evaluation.

$$C_2H_5OH + H_2O \rightarrow 2CO + 4H_2 \qquad \Delta H_{298K} = 256 \text{ kJ mol}^{-1} \qquad (4)$$

$$C_2H_5OH + 3H_2O \rightarrow 2CO_2 + 6H_2 \qquad \Delta H_{298K} = 174 \text{ kJ mol}^{-1} \qquad (5)$$

On the other hand, other products are observed in Figure 3 because the consumption of water does not follow the complete conversion of ethanol. This phenomenon points to reactions involving the decomposition of ethanol. The decomposition of ethanol can also form the synthesis gas (eq. 6). The methane produced in eq. 6 can be further decomposed to hydrogen and carbon (eq. 7). The ethane and ethylene can be produced from the dehydration of ethanol (eq. 8), while oxygenates such as acetaldehyde might be formed from the dehydrogenation of ethanol (eq. 9).

$$C_2H_5OH \rightarrow CH_4 + CO + H_2 \qquad \Delta H_{298K} = 49 \text{ kJ mol}^{-1} \qquad (6)$$

$$CH_4 \rightarrow C_{(S)} + 2H_2 \qquad \Delta H_{298K} = 75 \text{ kJ mol}^{-1} \qquad (7)$$

$C_2H_5OH \rightarrow C_2H_4 + H_2O$ $\Delta H_{298K} = 45$ kJ mol^{-1} (8)

$C_2H_5OH \rightarrow CH_3CHO + H_2$ $\Delta H_{298K} = 68$ kJ mol^{-1} (9)

Table 2 summarises the results collected after 4 h of the steam reforming of ethanol at 600°C. The DTA peaks related to the oxidation of carbon and the mass of carbon formed per mass of catalyst ($m_C\ m_{cat}^{-1}$) estimated by the TPO/DTA analyses of spent catalysts are also shown in Table 2.

Table 2. Results of the steam reforming of ethanol after 4 h and TPO/DTA data

Sample	X_{H2O} (%)	X_{ET} (%)	S_{CO} (%)	S_{H2} (%)	H_2/CO ratio (mol mol^{-1})	TPO/DTA analysis	
						$m_C\ m_{cat}^{-1}$ ($g_C\ g_{cat}^{-1}$)	DTA Peak (°C)
Fe66	73	100	49	88	2.7	0.08	581
Fe75	68	100	45	79	2.7	0.27	561
Fe80	14	26	10	54	6.0	0.04	514
CuFe70	48	72	38	70	2.6	0.05	528
CoFe70	86	100	60	95	2.6	0.01	539

(EtOH:H_2O = 1 mol mol^{-1}; W_{CAT} = 0.1 g; T_{REA} = 600°C, F_{LIQ} = 0.5 mL h^{-1}).

The selectivity towards both the components of the synthesis gas and the water consumption decreases with increasing Fe/Al ratio. Therefore, the performance of these Fe-Al samples followed the specific surface area measurements in this reaction (Table 1). This worsening in the performance for samples with increasing Fe/Al ratio is more evident taking into account the results collected for the Fe80 catalyst. This sample exhibited low conversion of ethanol in addition to the lowest values for water consumption and selectivity.

The TPO/DTA analysis revealed lower amount of coke on the Fe66 sample compared to the Fe75 catalyst. This result is in agreement with the higher consumption of water and selectivity towards H_2 and CO observed for the Fe66 sample because coke might be gasified by water to generate synthesis gas (eq. 10). However, this sample might require approximately 20°C higher temperatures for its regeneration compared to the Fe75 catalyst.

$C_{(S)} + H_2O \rightarrow CO + H_2$ $\Delta H_{298K} = 131$ kJ mol^{-1} (10)

Regarding the samples in which 10 mol. % of iron was substituted by copper or cobalt, Table 2 shows that the modification leads to a significant improvement on the activity and the selectivity towards the synthesis gas after 4 h of reaction. This improvement on the performance is expected from the changes on the structure of the materials provided by the divalent metal (Cu^{2+} and Co^{2+}), which leaded to an increase in the specific surface area (Table 1), crystallites of iron oxides with smaller diameters (Figure 2-a) and higher thermal stability ascribed to the mixed oxides (Vaccari, 1998). Moreover, it is expected from previous results collected for the decomposition of ethanol (Souza *et al.*, 2012) and to the higher activity for the reforming reactions of Co compared to Fe (Jones *et al.*, 2008). The H_2/CO ratio of the synthesis gas is the same for the CuFe70 and CoFe70 samples and is almost at the same level compared to the Fe66 and Fe75 catalysts. The low formation of carbon on the modified samples compared to the other samples with different Fe/Al is remarkable. The CoFe70 catalyst exhibited the best performance because this sample showed the highest consumption of water, selectivity towards both the H_2 and CO products and formed the lowest quantity of coke.

Figure 4-a shows the evolution of the conversion of ethanol and consumption of water with time on stream for the Fe80, CuFe70 and CoFe70 catalysts. The corresponding selectivity towards H_2 and CO with time on stream is showed in Figure 4-b. Figure 4-a depicts the deactivation phenomenon that takes place on the Fe80 catalyst. The conversion of ethanol and the water consumption decrease continuously after 1 h of reaction for the Fe80 catalyst, thus revealing low thermal stability for this sample. The selectivity towards H_2 and CO in Figure 4-b follows this behaviour for the Fe80 catalyst.

As previously showed in Table 2, the overall performance is enhanced when Fe is partly substituted by Cu or Co. Comparing to the Fe80 sample, the modification with copper enhances the activity (Figure 4-a) and the selectivity towards H_2 and CO (Figure 4-b) of the sample with time on stream. Despite exhibiting the same trend, the decrease on the activity during the reaction is less dramatically for the CuFe70 sample compared to the Fe80 catalyst. The performance for the CuFe70 might be affected by the sintering of the Cu^0 phase, because the reduction of the CuO phase takes place at low temperatures (Figure 2-b), as this phenomenon was observed after decomposition of ethanol over Cu-Ni-Al samples (de Souza *et al.*, 2012b). In addition to the higher values, the Figure 4-a and Figure 4-b show that both the conversions and the distribution of products remain at the same level with time on stream for the CoFe70 catalyst. Therefore, Figure 4-a and Figure 4-b point to the high thermal stability for this sample in addition to its best activity and selectivity results.

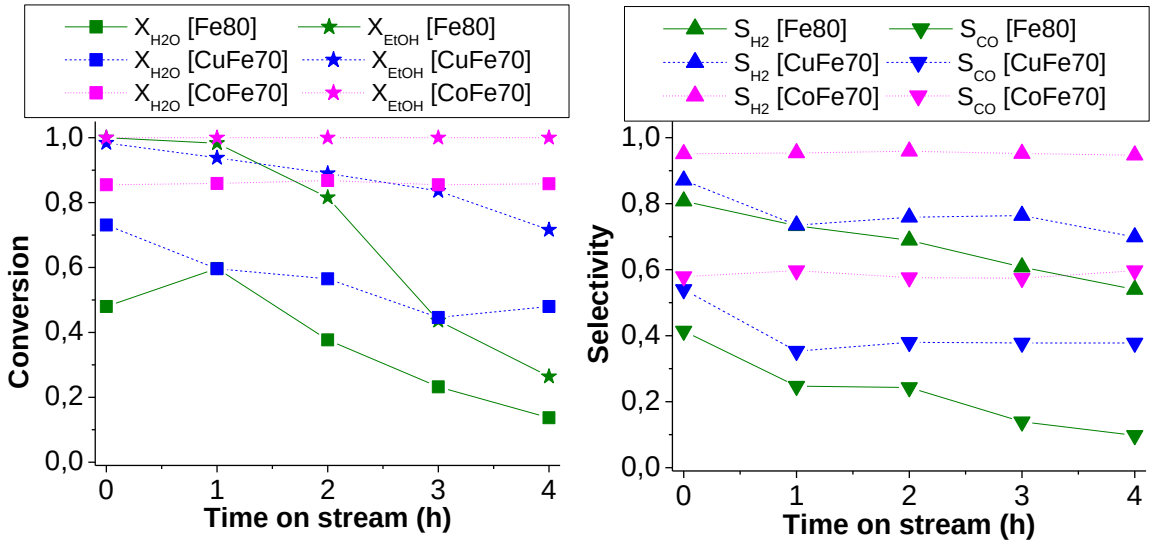

(a) (b)

Figure 4. Evolution of (a) the ethanol conversion and water consumption and (b) the selectivity towards H_2 and CO with time on stream for the steam reforming of ethanol over the Fe80 (solid line), CuFe70 (dash) and CoFe70 (dot) catalysts

4 Conclusions

A series of Fe-Al samples with different Fe/Al ratios and modified with Cu or Co was prepared by the precipitation method, characterised and evaluated for the steam reforming of ethanol. Higher specific surface areas and easier reducible iron species were observed for samples with lower Fe/Al ratio and for samples modified with Cu or Co. The former samples also exhibited smaller crystallites of iron oxides. These changes on the structure provided higher conversions of ethanol and water consumption and higher selectivity towards H_2 and CO for the samples with lower Fe/Al ratios and for the modified catalysts. The Co-loaded sample showed the best performance in terms of activity, selectivity and formation of coke. The results obtained point to the investigation of Cu- or Co-promoted samples with lower Fe/Al ratios.

Acknowledgements
The authors wish to thank the financial support and scholarships granted by the "Conselho Nacional de Desenvolvimento Científico e Tecnológico – CNPq" and by the "Coordenação de Aperfeiçoamento de Pessoal de Nível Superior – CAPES".

References

Cai W.-J., Qian L.-P., Yue B., Chen X.-Y. and He H.-Y. (2013), Reforming of CH_4 with CO_2 over Co/Mg–Al oxide catalyst, *Chinese Chemical Letters*, **24**, 777-779.

Coronel L., Múnera J.F., Tarditi A.M., Moreno M.S. and Cornaglia L.M. (2014), Hydrogen production by ethanol steam reforming over Rh nanoparticles supported on lanthana/silica systems, *Applied Catalysis B: Environmental*, **160–161**, 254-266.

Crepaldi E.L., Pavan P.C. and Valim J.B. (2000), Comparative study of the coprecipitation methods for the preparation of Layered Double Hydroxides, *Journal of the Brazilian Chemical Society*, **11**, 64-70.

Davidson S., Sun J. and Wang Y. (2013), Ethanol Steam Reforming on Co/CeO_2: The Effect of ZnO Promoter, *Topics in Catalysis*, **56**, 1651-1659.

de Souza G., Ávila V.C., Marcílio N.R. and Perez-Lopez O.W. (2012a), Synthesis Gas Production by Steam Reforming of Ethanol over M-Ni-Al Hydrotalcite-type Catalysts; M = Mg, Zn, Mo, Co, *Procedia Engineering*, **42**, 1805-1815.

de Souza G., Balzaretti N.M., Marcílio N.R. and Perez-Lopez O.W. (2012b), Decomposition of Ethanol Over Ni-Al Catalysts: Effect of Copper Addition. *Procedia Engineering*, **42**, 335-345.

Dias J.A.C. and Assaf J.M. (2003) Influence of calcium content in $Ni/CaO/\gamma\text{-}Al_2O_3$ catalysts for CO_2-reforming of methane, *Catalysis Today*, **85**, 59-68.

Dry M.E. (2002), The Fischer-Tropsch process: 1950-2000, *Catalysis Today*, **71**, 227-241.

Escobar C. and Perez-Lopez O. (2014), Hydrogen Production by Methane Decomposition Over Cu–Co–Al Mixed Oxides Activated Under Reaction Conditions, *Catalysis Letters*, **144**, 796-804.

Espinal R., Taboada E., Molins E., Chimentao R.J., Medina F. and Llorca J. (2012), Cobalt hydrotalcites as catalysts for bioethanol steam reforming. The promoting effect of potassium on catalyst activity and long-term stability, *Applied Catalysis B: Environmental*, **127**, 59-67.

Fakeeha A.H., Naeem M.A., Khan W.U. and Al-Fatesh A.S. (2014), Syngas production via CO_2 reforming of methane using Co-Sr-Al catalyst, *Journal of Industrial and Engineering Chemistry*, **20**, 549-557.

Frost R.L., Musumeci A.W., Bostrom T., Adebajo M.O., Weier M.L. and Martens W. (2005), Thermal decomposition of hydrotalcite with chromate, molybdate or sulphate in the interlayer, *Thermochimica Acta*, **429**, 179-187.

Galvita V.V., Semin G.L., Belyaev V.D., Semikolenov V.A., Tsiakaras P. and Sobyanin V.A. (2001), Synthesis gas production by steam reforming of ethanol, *Applied Catalysis A-General*, **220**, 123-127.

González Vargas O.A., de los Reyes Heredia J.A., Wang J.A., Chen L.F., Montesinos Castellanos A. and Llanos M.E. (2013), Hydrogen production over Rh/Ce-MCM-41 catalysts via ethanol steam reforming, *International Journal of Hydrogen Energy*, **38**, 13914-13925.

Hayakawa H., Tanaka H. and Fujimoto K. (2006), Studies on precipitated iron catalysts for Fischer-Tropsch synthesis, *Applied Catalysis A-General*, **310**, 24-30.

Hermes, N.A. (2010), *Hidrogênio e nanotubos de carbono por decomposição catalítica do metano: desempenho de catalisadores à base de cobalto e alumínio*. MSc. Thesis. UFRGS, Porto Alegre.

Hermes N.A., Lansarin M.A. and Perez-Lopez O.W. (2011), Catalytic Decomposition of Methane Over M-Co-Al Catalysts (M = Mg, Ni, Zn, Cu), *Catalysis Letters*, **141**, 1018-1025.

Huber G.W., Chheda J.N., Barrett C.J. and Dumesic J.A. (2005), Production of liquid alkanes by aqueous-phase processing of biomass-derived carbohydrates, *Science*, **308**, 1446-1450.

Jones G., Jakobsen J.G., Shim S.S., Kleis J., Andersson M.P., Rossmeisl J., Abild-Pedersen F., Bligaard T., Helveg S., Hinnemann B., Rostrup-Nielsen J.R., Chorkendorff I., Sehested J. and Nørskov J.K. (2008), First principles calculations and experimental insight into methane steam reforming over transition metal catalysts, *Journal of Catalysis*, **259**, 147-160.

Li W., Wang H., Ren Z., Wang G. and Bai J. (2008), Co-production of hydrogen and multi-wall carbon nanotubes from ethanol decomposition over Fe/Al_2O_3 catalysts, *Applied Catalysis B-Environmental*, **84**, 433-439.

Lira E., Lopez C.M., Oropeza F., Bartolini M., Alvarez J., Goldwasser M., Linares F.L., Lamonier J.-F. and Zurita M.J.P. (2008), HMS mesoporous silica as cobalt support for the Fischer-Tropsch Synthesis: Pretreatment, cobalt loading and particle size effects, *Journal of Molecular Catalysis A-Chemical*, **281**, 146-153.

Oliveira A.C. and Rangel M.d.C. (2003), Desidrogenação do etilbenzeno sobre compostos de ferro e alumínio, *Química Nova*, **26**, 170-176.

Palmer S.J., Spratt H.J. and Frost R.L. (2009), Thermal decomposition of hydrotalcites with variable cationic ratios, *Journal of Thermal Analysis and Calorimetry*, **95**, 123-129.

Ponton Lozano S., Montoya Gómez N.Y., Martínez Sepúlveda J.A., Cañizares Cañizares P. and Fernández Morales F.J. (2014), Study of pre-treatments for an enhanced bio-ethanol production from the organic fraction of municipal solid wastes, *Global NEST Journal*, **16**

Rostrup-Nielsen J.R. (2005), Making fuels from biomass, *Science*, **308**, 1421-1422.

Song L.X., Chen J., Zhu L.H., Xia J. and Yang J. (2011), Modification in Structure, Phase Transition, and Magnetic Property of Metallic Gallium Driven by Atom–Molecule Interactions, *Inorganic Chemistry*, **50**, 7988-7996.

Souza G., Ruoso C., Balzaretti N.M., Marcilio N.R. and Perez-Lopez O.W. (2012), Synthesis gas and carbon nanotubes production from catalytic decomposition of renewable resources. *Proceedings Venice 2012, Fourth International Symposium on Energy from Biomass and Waste* (ed by, p. PG09. San Servolo - Venice.

Vaccari A. (1998), Preparation and catalytic properties of cationic and anionic clays, *Catalysis Today*, **41**, 53-71.

Wan H., Wu B., Zhang C., Xiang H. and Li Y. (2008), Promotional effects of Cu and K on precipitated iron-based catalysts for Fischer-Tropsch synthesis, *Journal of Molecular Catalysis A-Chemical*, **283**, 33-42.

Wang G., Wang H., Li W., Ren Z., Bai J. and Bai J. (2011), Efficient production of hydrogen and multi-walled carbon nanotubes from ethanol over Fe/Al_2O_3 catalysts, *Fuel Processing Technology*, **92**, 531-540.

Wang W. and Wang Y. (2010), Steam reforming of ethanol to hydrogen over nickel metal catalysts, *International Journal of Energy Research*, **34**, 1285-1290.

Zhang B., Cai W., Li Y., Xu Y. and Shen W. (2008a), Hydrogen production by steam reforming of ethanol over an Ir/CeO_2 catalyst: Reaction mechanism and stability of the catalyst, *International Journal of Hydrogen Energy*, **33**, 4377-4386.

Zhang C.H., Yang Y., Teng B.T., Li T.Z., Zheng H.Y., Xiang H.W. and Li Y.W. (2006), Study of an iron-manganese Fischer-Tropsch synthesis catalyst promoted with copper, *Journal of Catalysis*, **237**, 405-415.

Zhang L., Li W., Liu J., Guo C., Wang Y. and Zhang J. (2009a), Ethanol steam reforming reactions over $Al_2O_3{\cdot}SiO_2$-supported Ni–La catalysts, *Fuel*, **88**, 511-518.

Zhang L., Millet J.-M.M. and Ozkan U.S. (2009b), Effect of Cu loading on the catalytic performance of Fe-Al-Cu for water-gas shift reaction, *Applied Catalysis A-General*, **357**, 66-72.

Zhang L.H., Xiang X., Zhang L., Li F., Zhu J., Evans D.G. and Duan X. (2008b), Influence of iron substitution on formation and structure of Cu-based mixed oxides derived from layered double hydroxides, *Journal of Physics and Chemistry of Solids*, **69**, 1098-1101.